Experimental and finite element analysis of the mouse caudal vertebrae loading model: prediction of cortical and trabecular bone adaptation

Biomech Model Mechanobiol (2012) 11:221–230
DOI 10.1007/s10237-011-0305-3

ORIGINAL PAPER

Experimental and finite element analysis of the mouse caudal vertebrae loading model: prediction of cortical and trabecular bone adaptation

D. Webster · A. Wirth · G. H. van Lenthe · R. Müller

Received: 19 December 2010 / Accepted: 19 March 2011 / Published online: 7 April 2011

Abstract In this study, we attempt to predict cortical and trabecular bone adaptation in the mouse caudal vertebrae loading model using knowledge of bone's local mechanical environment at the onset of loading. In a previous study, we demonstrated appreciable 25.9 and 11% increases in both trabecular and cortical bone volume density, respectively, when subjecting the fifth caudal vertebrae (C5) of C57BL/6 (B6) mice to an acute loading regime (amplitude of 8N, 3000 cycles, 10 Hz, 3 times a week for 4 weeks). We have also established a validated finite element (FE) model of the C5 vertebra using micro-computed tomography (micro-CT), which characterizes, in 3D, the micro-mechanical strains present in both cortical and trabecular compartments due to the applied loads. To investigate the relationship between load-induced bone adaptation and mechanical strains in-vivo and in-silico data sets were compared. Using data from the previous cross-sectional study, we divided cortical and trabecular compartments into 15 subregions and determined, for each region, a bone formation parameter ΔBV/BS (a cross-sectional measure of the bone volume added to cortical and trabecular surfaces following the described loading regime). Linear regression was then used to correlate mean regional values of ΔBV/BS with mean values of mechanical strains derived from the FE models which were similarly regionalized. The mechanical parameters investigated were strain energy density (SED), the orthogonal strains (e_x, e_y, e_z) and the three shear strains (e_{xy}, e_{yz}, e_{zx}). For cortical regions, regression analysis showed SED to correlate extremely well with ΔBV/BS ($R^2 = 0.82$) and e_z ($R^2 = 0.89$). Furthermore, SED was found to predict expansion of the cortical shell correlating significantly with the regional percentage increases in cortical tissue volume ($R^2 = 0.92$), cortical marrow volume ($R^2 = 0.91$) and cortical thickness ($R^2 = 0.56$). For trabecular regions, FE parameters were found not to correlate with load-induced trabecular bone morphology. These results indicate that load-induced cortical morphology can be predicted from population data, whereas the prediction of trabecular morphology requires subject-specific micro-architecture.

Keywords Mechanical loading · Cortical bone · Trabecular bone · Bone adaptation

D. Webster · A. Wirth · G. H. van Lenthe · R. Müller (✉)
Institute for Biomechanics, ETH Zürich,
Wolfgang-Pauli-Strasse 10, 8093 Zürich, Switzerland
e-mail: ram@ethz.ch
URL: http://www.biomech.ethz.ch

1 Introduction

Osteoporosis is a disease characterized by an excessive decrease in bone mass which can lead to skeletal fragility and an increased susceptibility to fractures, dramatically reducing a person's quality of life and in some cases leading to morbidity. In 2000, the number of osteoporotic fractures was estimated at 3.79 million (Johnell and Kanis 2006). The total direct costs were estimated at €31.7 billion, a figure which is expected to increase to €76.7 billion (Kanis and Johnell 2005). In view of these statistics, there is clearly a need to prevent osteoporotic fractures. In clinical practice, current fracture predictions are based on the mineral content of bone at a particular instant and do not account for the adaptations, which will occur over time. The prediction of fracture risk could therefore be under- or over estimated thereby leading to inaccurate prognoses and unnecessary costs. The mechanical environment of both cortical and trabecular bone is a primary determinant of bone adaptation (Duncan and Turner 1995; Marcus 1995; Biewener, Fazzalari et al. 1996; Evans 1998). The ability to incorporate this dynamic information

in fracture prediction models could therefore dramatically improve accuracy. Today, using micro-finite element analysis (μFE) (Müller and Rüegsegger 1995), it is possible to compute the micro-structural stresses and strains in both cortical and trabecular components of bone at a given time point. However, it is not yet fully understood how this 'initial' mechanical environment determines subsequent cortical and trabecular adaptation. Furthermore, if this was known, it would be equally important to establish whether population- or patient-specific bone architectures would be required since this would shape the strategies applied in a clinical setting. For example, if patient-specific bone architectures were required, imaging technologies capable of resolving a person's bone micro-architecture, in-vivo, would be essential. If not, cadaver scans could be used to construct databases containing a range of geometries representative of particular populations. The latter option being, perhaps, the preferable option owing to smaller operational costs, in addition to being free from health issues related to X-ray dosage. With this in mind, the aims of this study are to address two specific questions: Firstly, can an 'initial' mechanical environment predict subsequent cortical and trabecular adaptation? Secondly, is it sufficient to base predictions on an average, 'initial' mechanical environment derived from a group of geometrically similar bones? To answer these questions, we apply a combined experimental and computational approach using the mouse caudal vertebra loading model.

Recently, we established an in vivo loading model for both cortical and trabecular bone adaptation using C57BL/6 (B6) female mice (Webster, Wasserman et al. 2010). By mechanically stimulating the fifth caudal vertebra (C5), we were able to demonstrate a significant load affect in both cortical and trabecular components. Following bouts of mechanical stimulation (amplitude: 8N, frequency: 10 Hz, number of cycles: 3000, 3 times per week for a period of 4 weeks), cortical and trabecular bone volume was shown to increase significantly by 11 and 23%, respectively, when measured using micro-computed tomography (micro-CT). Furthermore, we have also developed and validated a micro-finite element (μFE) model of the loaded C5 caudal vertebrae (Webster, Morley et al. 2008). An opportunity therefore exists to investigate the feasibility of using the 'initial' mechanical environment to predict subsequent cortical and trabecular morphology. Furthermore, owing to the cross-sectional nature of the in-vivo study, an opportunity also exists to assess the possibility of predictions based on 'population' data. In the paper presented here, we therefore correlate μFE models of C5 vertebrae from groups of mice sacrificed before loading with load-induced bone formation as quantified by groups sacrificed after mechanical loading. In doing so, we hypothesize that knowledge of the 'initial' mechanical environment (averaged over a group representing the geometric state of bone architecture before loading) is sufficient to predict average, load-induced increases in cortical and trabecular morphology.

2 Materials and methods

In a recent cross-sectional loading study (Webster, Wasserman et al. 2010), the fifth caudal vertebrae of female C57BL/6 mice (B6) were mechanically stimulated using a specially developed loading device. The loading device is able to cyclically compress the C5 vertebra via two stainless steel pins inserted into the adjacent C4 and C6 vertebrae. In the aforementioned study, groups of mice had stainless steel pins surgically inserted at 12 weeks of age. At 15 weeks of age, loading trials commenced: One group of mice ($B6_{8N}$) was subjected to a dynamic loading regime consisting of 3000 cycles per day, 3 days per week for 4 weeks (amplitude: 8N, frequency: 10 Hz). To quantify load-induced bone mass, a sham group ($B6_{0N}$) was fitted into the device for the same amount of time but received no mechanical stimulation. Both sham and the loaded groups were sacrificed at 19 weeks of age. To quantify age-related changes in bone mass throughout the 4 weeks of loading, a third group ($B6_{T0}$) was killed just before loading commenced (at 15 weeks of age). Results of this study showed that trabecular and cortical bone volume (Ct.BV and Tb.BV) increased, significantly by 23 and 11%, respectively (Webster, Wasserman et al. 2010). Furthermore, no significant age-related changes in bone architecture were detected.

In the study presented here, we assess the potential of the mechanical environment to predict subsequent bone adaptation by comparing μFE models of caudal vertebrae, prior to loading, with a measure of bone formation as previously quantified by micro-computed tomography (micro-CT). This comparison is facilitated by dividing the caudal vertebrae into overlapping regions (Fig. 1) and quantifying, for each region: (i) average mechanical tissue strains, (ii) a relevant measure of load-induced bone formation, and (iii) increases in structural parameters such as cortical and trabecular thickness. In doing so, profiles describing the variation of mechanical strains and bone forming activity throughout cortical and trabecular components can be constructed and directly compared.

2.1 Construction of the mechanical strain profile

To determine the micro-mechanical environment induced by the applied loads, micro-CT images of the vertebra belonging to the $B6_{T0}$ group were converted into 3D μFE models by mapping each bone voxel to an eight-node brick element. To model the intervertebral discs, additional voxels were added to the proximal and distal ends of the vertebra such that the disc's geometry was approximated (Sarver and Elliott 2005)

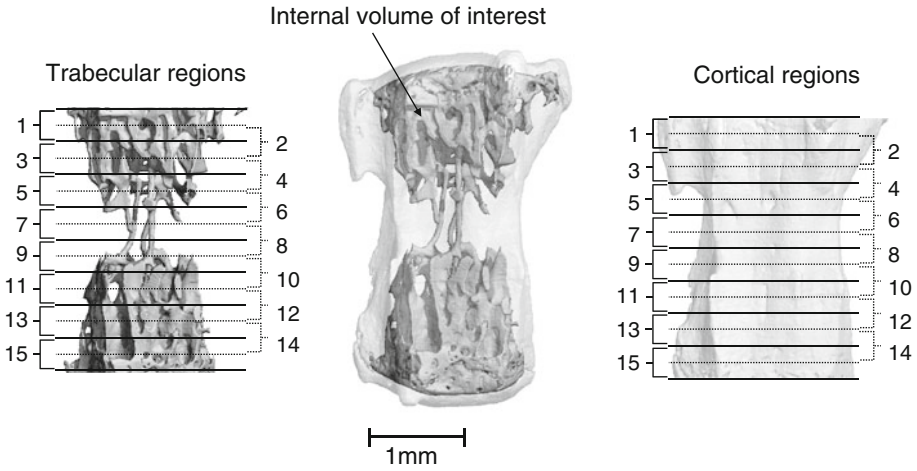

Fig. 1 Digital image of a whole B6 vertebra (C5) showing cortical and trabecular compartments which are subdivided into 15 overlapping regions (1–15)

yielding models consisting of approximately 1,800,000 elements. Following previous validation of this FE model (Webster, Morley et al. 2008), an initial value of 14.8 GPa was assigned as the Young's modulus to those voxels representing bone (Somerville, Aspden et al. 2004), and 2.48 MPa was given to those voxels describing the intervertebral disc (Sarver and Elliott 2005). Both materials had a Poisson's ratio of 0.3. All models were aligned in the z-axis. The z-axis corresponded to the proximal-distal direction of the tail, the x-axis corresponded to the medial-lateral direction, whilst the y-axis was defined by the ventral–dorsal direction. To mimic the loading conditions applied in-vivo, the surface of the proximal intervertebral disc was fixed in the axial direction while allowing free lateral movement. A compressive axial force was then applied to the surface of the distal intervertebral disc (Fig. 2). The FE model and the accompanying boundary conditions were previously validated (Webster, Morley et al. 2008). Briefly, following the excision and pinning of mouse tails, micro-strain gages were attached to ventral and dorsal periosteal surfaces of C5 vertebrae. Upon loading the pinned mouse tails, mechanical strains were recorded and compared with the strains determined by FE models. Strong agreements were found ($R^2 > 0.96$). To enable the economical use of computer memory, FE models were solved using an element-by-element method (Smith and Griffiths 1998; Boyd, Müller et al. 2002) running on a super computer (CSCS, Manno, Switzerland) consisting of 8 IBM Regatta p690 SMPs for a total of 256 Power4 CPUs. To construct the profile which describes the variation of mechanical strains throughout the vertebra, bone tissue strains were extracted from the elements constituting the predefined cortical and trabecular regions. Average strains for each region were then determined. The regions (Fig. 1) were defined by first determining the length of cortical bone, which ran along the z-axis (proximal-distal) of the vertebrae. This was found to span the loci defining the upper and lower 15% of a vertebra. This section of cortical bone was then subdivided into 15

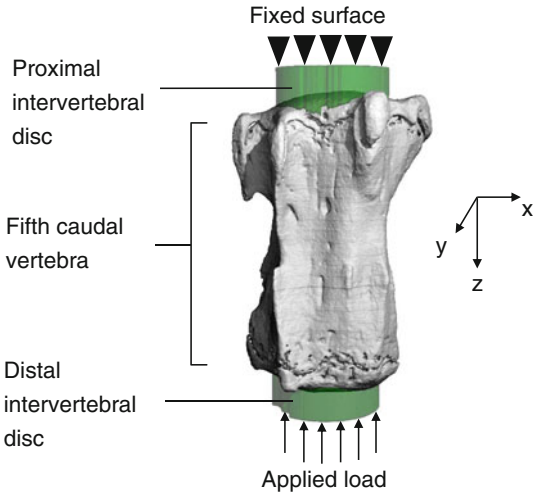

Fig. 2 Diagram showing the FE model. Thresholded μCT images of the C5 vertebrae were aligned in the z-axis, and additional voxels were created to model the intervertebral discs. Load was applied to the distal surface, whilst the proximal end was fixed in the z-direction allowing free lateral movement

overlapping regions: 8 distinct regions, each with the same field depth, and 7 overlapping regions, spanning consecutive midpoints of the aforementioned 8 regions. The trabecular regions of analysis were then defined by the loci of the cortical regions enclosing the trabecular bone. The mechanical parameters analysed for trabecular and cortical regions were the following: strain energy density (SED), orthogonal strains (e_x, e_y and e_z), and shear strains (e_{xy}, e_{yz}, e_{zx}). Paraview (Kitware Inc. New York) was used to visualize the spatial distribution of mechanical strains.

2.2 Construction of the load-induced bone formation profile

Bone morphometry was previously assessed using micro-computed tomography with 5 times frame averaging (6 µm voxel size, 50 kVp, 160 µA, Scanco Medical AG Switzerland). The vertebrae belonging to groups $B6_{T0}$, $B6_{0N}$ and

$B6_{8N}$ were subdivided into cortical and trabecular regions as previously outlined, where the heights of the vertebrae belonging to $B6_{T0}$ were not significantly different to the more mature groups $B6_{0N}$ and $B6_{8N}$. Morphometric parameters specific to cortical and trabecular regions were then determined using a direct 3D approach (Hilderbrand 1999; Bouxsein, Boyd et al. 2010), these included cortical bone surface (Ct.BS), cortical bone volume (Ct.BV), cortical tissue volume (Ct.TV), cortical marrow volume (Ct.MV), cortical thickness (Ct.Th), cortical cross-sectional area (Ct.T.Ar), trabecular bone surface (Tb.BS), trabecular bone volume (Tb.BV), trabecular thickness (Tb.Th) and trabecular number (Tb.N). To provide a measure of load-induced bone formation from the cross-sectional data available, the parameter ΔBV/BS was calculated for both cortical (Ct.ΔBV/BS) and trabecular (Tb.ΔBV/BS) bone. This was determined by calculating, for each region, the difference in mean bone volume between the groups loaded at 8 and 0N. The regional ΔBV's were then normalized by the mean regional values for bone surface area (BS) specific to the $B6_{T0}$ group. ΔBV/BS can therefore be thought of as a cross-sectional measure of the amount of new bone which is deposited, due to a load of 8N, onto the bone surface available at the start of loading. In addition to the ΔBV/BS, profiles for mean percentage increase in Ct.TV (ΔCt.TV), Ct.MV (ΔCt.MV), Ct.Th (ΔCt.Th), Ct.T.Ar (ΔCt.T.Ar), Tb.Th (ΔTb.Th), and Tb.N (ΔTb.N) were calculated from $B6_{0N}$ and $B6_{8N}$ groups.

2.3 Statistical analysis

To investigate the relationship between the micromechanical environment and load-induced bone adaptation, linear regression was used to test for correlations between the different sets of regional profiles defined for cortical and trabecular bone, i.e., the mechanical parameter profiles, ΔBV/BS profiles and those profiles describing the percentage increase in structural parameters (i.e. ΔCt.TV, ΔCt.Th). For all statistical analyses, the GNU statistical package R (Version 2.5.1, http://www.r-project.org) was used.

3 Results

The morphological data used in this study were reported recently (Webster, Wasserman et al. 2010), in which C57BL/6 female mice were subjected to a dynamic loading regime (3000 cycles, 10 Hz, 3 times per week, for a duration of 4 weeks), and it was shown for those mice loaded with an amplitude of 8N ($B6_{8N}$ group) that Ct.BV, Ct.Th, Tb.BV and Tb.Th were 11, 5, 23 and 24% significantly higher ($P < 0.05$) when compared with the group which received no mechanical stimulation ($B6_{0N}$ group).

3.1 The micro-mechanical environment

Mechanical strain profiles for the cortical component of the C5 caudal vertebrae (Fig. 3a) reveal that compressive axial strain magnitudes are superior to both the orthogonal and shear strain magnitudes, which occur in other planes. The maximum mean compressive strain is shown to occur local to the centre of the vertebrae (Fig. 3a, region 7, 885 $\mu\varepsilon$). All cortical regions are subject to similar levels of positive strain ($\approx 200\,\mu\varepsilon$) in the x–y plane, whilst mean shear strain values in all three orthogonal planes are close to $0\,\mu\varepsilon$. Analysis of the mean strains for trabecular bone shows that the trabecular network is predominantly in a state of compression where regional mean, axial compressive strains reach −842 and $-709\,\mu\varepsilon$ in both proximal and distal regions (Fig. 3b, regions 3 and 14). Minimum mean trabecular compressive strains occur local to the centre of the vertebrae ($-367\,\mu\varepsilon$, region 7). Note that the standard errors displayed in Fig. 3a, b describe the variation of the mean mechanical parameter across the analysed group of C5 vertebrae ($n = 10$) and not the variation of mechanical strains across all of the finite elements constituting the defined regions. Inspection of the orthogonal strains e_x and e_y shows that positive strains occur in the trabecular network in the plane transverse to the direction of loading where maximum values of e_x and e_y occur in proximal and distal regions (Fig. 3b, regions 2 and 14). This is confirmed visually in Fig. 4. The small deviations of shear strain e_{xy} from zero indicate that there is little shearing of the trabecular network in the plane transverse to the direction of loading. Shearing is shown to be present, however, in central regions (Fig. 3b, regions 5–10), in planes parallel to the axial direction of loading, as demonstrated by the regional variation of e_{yz} and e_{zx}. Comparison of axial strain (e_z) values for both cortical and trabecular components reveals how the load is distributed between cortical and trabecular components. At distal and proximal regions, trabecular bone supports a larger proportion of the load whilst at central regions, most of the load is transferred through the cortical shell. The same is true of the regional variation in mean strain energy density (SED), Fig. 5.

3.2 Load-induced bone formation

Analysis of cortical bone shows the regional variation of Ct.ΔBV/BS to be almost parabolic in form (Fig. 6), having a peak value of $0.016\,mm^3/mm^2$ at region 7. Trabecular bone formation activity appeared to be highest in the most proximal and distal regions (Fig. 6), where an average of $0.011\,mm^3/mm^2$ and $0.015\,mm^3/mm^2$ of bone was deposited. At regions 9 and 10, a distinct lack of anabolic activity is apparent.

For cortical bone, linear regression showed significant correlations to exist between Ct.ΔBV/BS, ΔCt.TV, ΔCt.MV

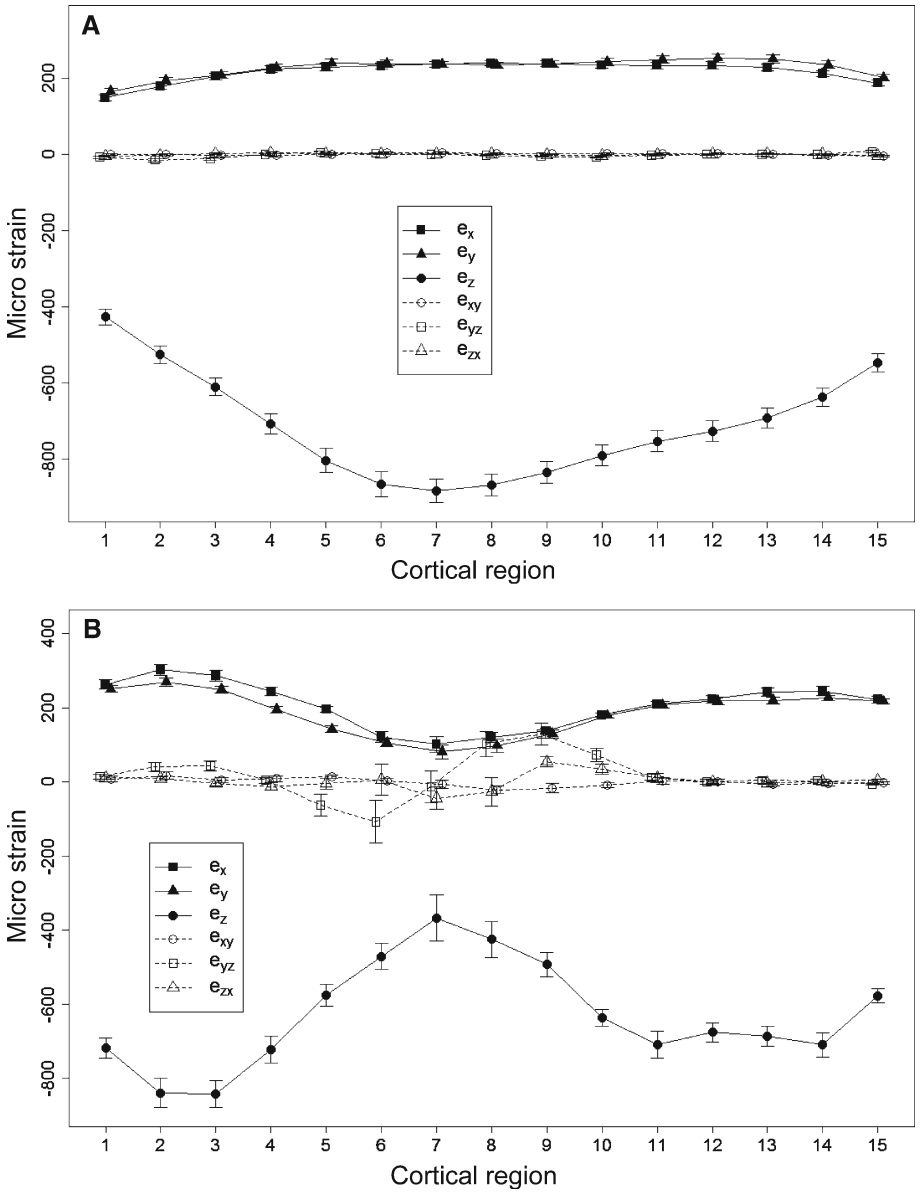

Fig. 3 Regional variation of mean mechanical strains ($e_x, e_y, e_z, e_{xy}, e_{yz}, e_{zx}$) for both cortical **a** and trabecular **b** bone. Standard errors are shown and describe the variation of the mean mechanical parameter across animals in group $B6_{T0}$

and ΔCt.Th ($R^2 = 0.81$ and 0.64, 0.21, respectively, $P < 0.05$, Fig. 7a–c). These data infer that the addition of new bone contributes to a structural expansion of the cortical shell in the plane transverse to the direction of loading. Close inspection of the plots also reveals that external and internal volumetric expansion appear to be the greatest in central cortical regions (regions 6–10), whilst in proximal and distal regions, volumetric changes are less. This regional pattern appears to be inverted when considering the regional profiles for ΔCt.Th (Fig. 7c). It appears that ΔCt.Th is greater at distal regions compared with central regions. These differing patterns suggest that cortical remodelling mechanisms are region specific, i.e., structural expansion increases progressively towards the centre, whilst thickening appears to increase towards both proximal and distal regions. When viewed in the light of the hour-glass shape of the caudal vertebrae (Figs. 1 and 2) and the fact that before loading the cortical shell is progressively thicker towards the centre (data not shown), these data describe a morphing of the vertebrae towards a more cylindrical format with a homogenous wall thickness. From an engineering perspective, this would clearly accommodate the optimal support of the applied axial loading configuration. The initial cortical bone surface for each region was also quantified and found to negatively correlate with Ct.ΔBV/BS ($R^2 = 0.86$), i.e., the lower the initial bone surface, the higher the bone formation. This can be explained by the fact that mechanical strains are higher in regions where the initial bone surface is lower owing to the hour-glass shape of the cortical shell (refer to the proceeding section).

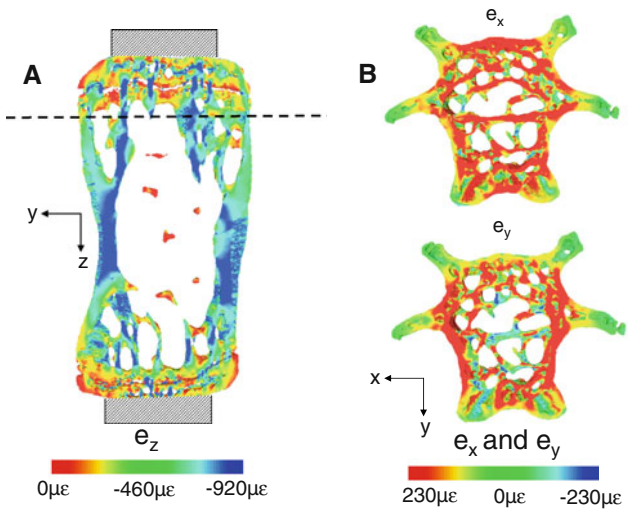

Fig. 4 **a** Visualization of a finite element simulation from one loaded vertebra. Axial strains in the y–z plane from one slice are shown. Dotted line shows the position from where the transverse x–y views are taken **b** Visualization of the positive strains which occur in the x–y plane

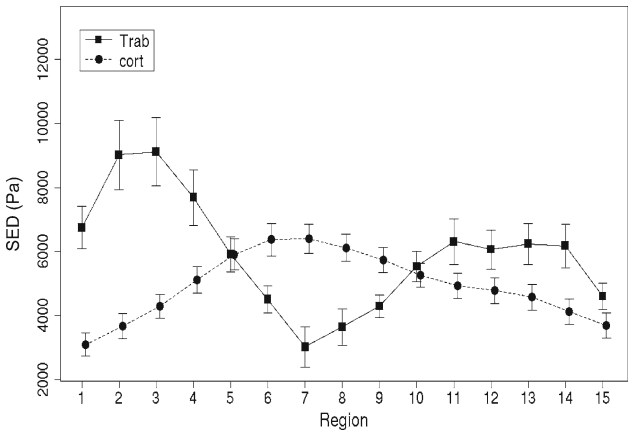

Fig. 5 Regional variation of the mean SED for both trabecular and cortical compartments. Standard errors are shown and describe the variation of the mean value of SED across animals in group $B6_{T0}$

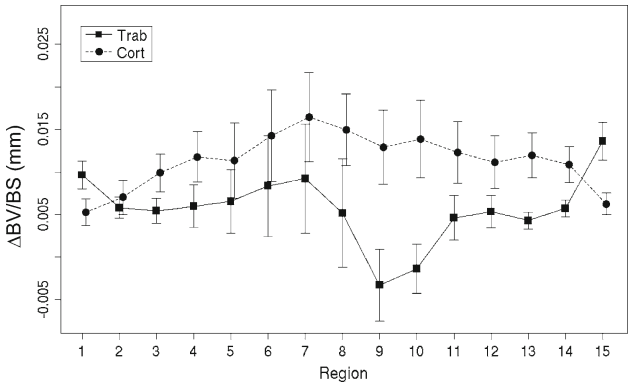

Fig. 6 Regional variation of ΔBV/BS for both cortical and trabecular bone. Standard errors are displayed

For trabecular bone, linear regression analysis shows that Tb.ΔBV/BS correlates significantly with ΔTb.Th ($R^2 = 0.79$, $P < 0.05$, Fig. 7e). A significant correlation is also shown to exist between Tb.ΔBV/BS and ΔTb.N ($R^2 = 0.26$, $P < 0.05$, Fig. 7f). Close inspection of the magnitude of changes for each region reveals no distinct patterns as was the case in cortical bone.

3.3 Relationship between the micro-mechanical environment and bone formation

Linear regression applied to the data sets describing mean regional bone formation in cortical bone and the corresponding mean mechanical parameters as determined by the FE model shows significant correlation to exist between, Ct.ΔBV/BS and SED ($R^2 = 0.82$, $P < 0.001$, Fig. 8). Ct.ΔBV/BS was also shown to correlate significantly with e_z ($R^2 = 0.89$, $P < 0.001$). When correlating the regional mechanical parameter profiles with those regional profiles describing the percentage increases in structural parameters, SED and e_z were found to predict the observed structural expansion of the cortical shell: SED significantly correlated with the ΔCt.TV ($R^2 = 0.92$, $P < 0.001$), ΔCt.MV ($R^2 = 0.91$, $P < 0.001$) and ΔCt.Th ($R^2 = 0.52$, $P < 0.001$). These same parameters were also found to correlate significantly with e_z ($R^2 = 0.90, 0.86$ and 0.33, respectively, $P < 0.01$).

For trabecular bone, no significant correlations were shown to exist between Tb.ΔBV/BS, e_x, e_y, e_z ($R^2 < 0.1$, $P > 0.05$) and SED (Fig. 8). Furthermore, no significant correlations existed when comparing the regional mechanical parameter profiles with regional percentage increases in ΔTb.Th and ΔTb.N.

4 Discussion

In the paper presented here, we correlated μFE models of C5 vertebrae from groups of mice sacrificed before loading with load-induced bone formation as quantified by groups sacrificed after mechanical loading. In doing so, we hypothesized that knowledge of the 'initial' mechanical environment, (averaged over a population representing the geometric state of bone architecture before loading), is sufficient to predict average, load-induced increases in cortical and trabecular morphology. The results presented here demonstrate that SED and axial strain values averaged over geometrically similar cortical architectures are able to predict the mean volumetric expansion and the mean cortical thickening observed in the previous loading study. These data confirm our hypothesis for cortical bone. The results pertaining to the cortical component of this study are in agreement with a different study carried out by Kotha et al. (Kotha, Hsieh et al. 2004).

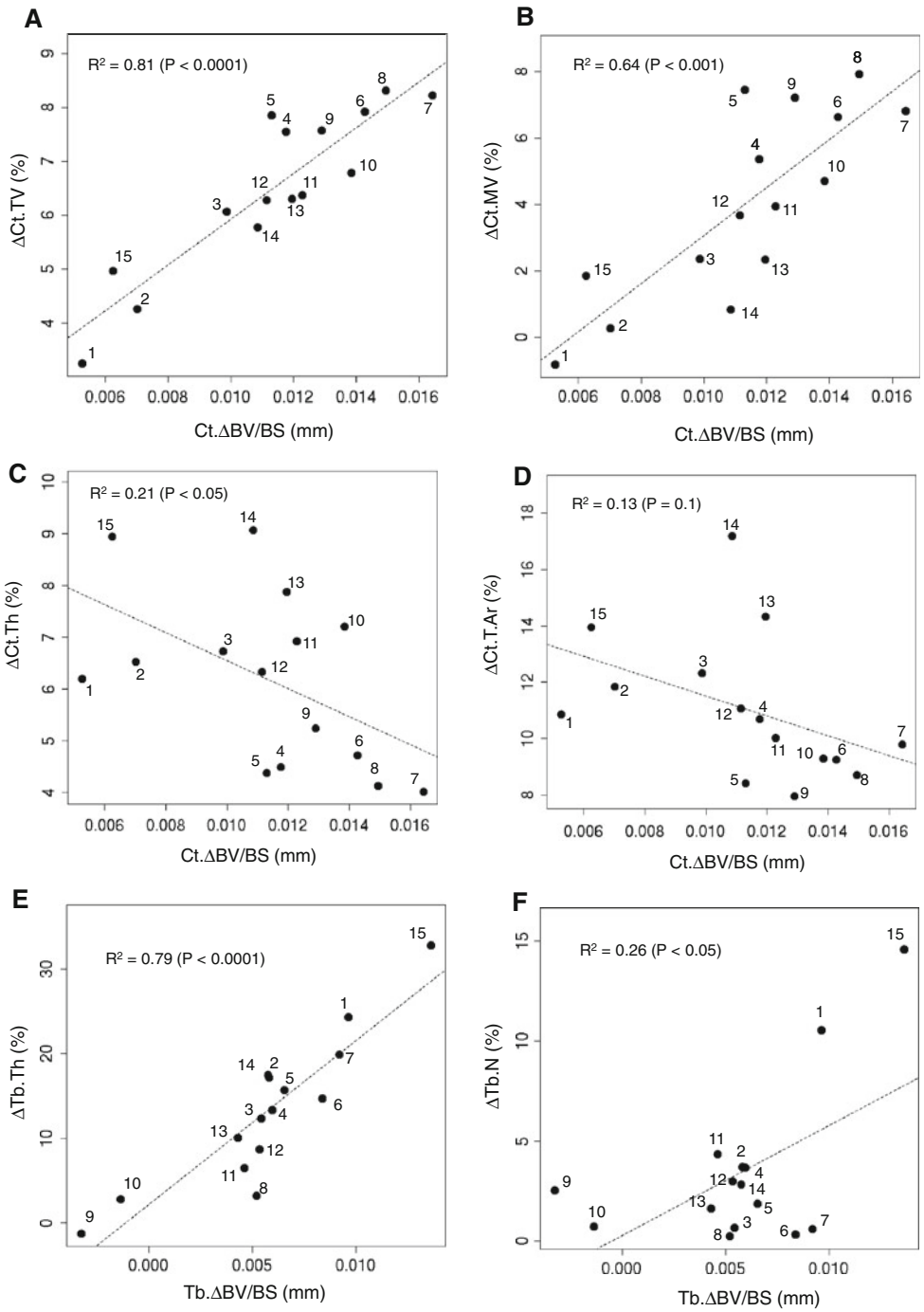

Fig. 7 Correlation of cortical and trabecular bone formation profiles (Ct.ΔBV/BS and Tb.ΔBV/BS) with regional percentage changes in cortical and trabecular structural indices: Ct.TV **a**, Ct.MV **b** Ct.Th **c** $Ct.T.Ar_{Ct}$ **d**, Tb.Th **e** and Tb.N **f**. The numbers shown next to the plotted points identify the region

Here, the authors employed a similar FE-based strategy using the rat ulnae model and found that both peak axial strains and peak SED at seven locations along the length of the ulna correlated with increases in bone mineral content ($R^2 = 0.89$ and 0.9, respectively).

For trabecular bone, the initial mechanical environment did not correlate with any aspect of load-induced increases in trabecular morphology. Our data show that there is clear response to mechanical loading via the thickening of existing trabeculae; however, knowledge of the 'initial' mechanical environment cannot predict the extent of this thickening throughout the trabecular network. One explanation for this could be the distribution of mechanical strains present in the different trabecular regions. These distributions are greater than those in cortical regions (Refer to representative error bars in Fig. 8); furthermore, in the case of SED, distributions are non-Gaussian (data not shown). It could therefore be hypothesized that the calculated mean values

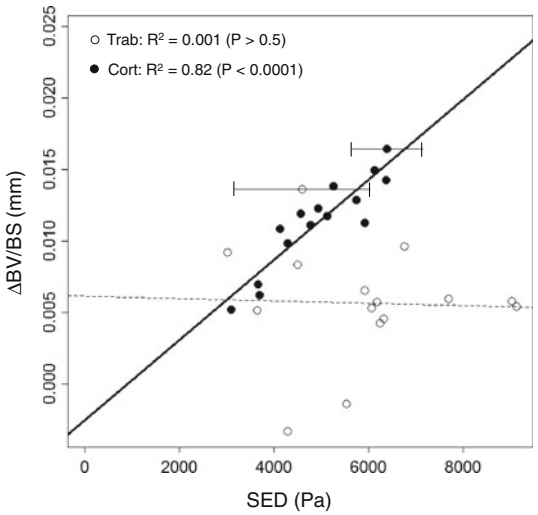

Fig. 8 Linear correlation of mean regional SED and mean regional ΔBV/BS for both trabecular and cortical bone. Error bars are representative of standard errors which describe the typical spread of SED throughout cortical and trabecular regions

are not representative of those responsible for load-induced bone formation. However, parametric studies which recomputed mean axial strains and mean SED's for different percentiles of the distributions (90th, 80th, 70th, etc.) yielded no improved correlations (data not shown). The most likely explanation for the poor correlations is the cross-sectional nature of the data. Even though trabecular bone mass is similar among mice, the spatial organization of the trabecular network is heterogeneous. Consequently, the distribution of mechanical strains throughout the trabecular network will be different for corresponding regions in each animal. This is illustrated by the standard errors associated with the SED profiles (Fig. 5) where it can be seen that inter-mouse variation of mean SED is larger in trabecular bone compared with that of cortical bone for certain regions. It, therefore, follows that any correlations, which exist between trabecular bone formation and the mechanical environment, are being obscured by statistical noise. The validity of this explanation is further reinforced when comparing this study with a study carried out by Kim et al. (Kim, Takai et al. 2003), who made similar correlations for trabecular bone but in a longitudinal fashion. Using the rat tail loading model (Guo, Eichler et al. 2002), the authors divided the trabecular compartment of loaded rat vertebrae into proximal, central and distal regions and correlated bone formation indices (as determined by histology) with average tissue SED values (as computed from FE models). Results revealed that bone formation rates correlated with average tissue strain energy density (SED) after one and two weeks of loading, $R^2 = 0.42$ and 0.37, respectively. To permit a longitudinal approach, FE models were derived from animals killed after they had received loading; thus, load-induced bone activity was not correlated with an 'initial' mechanical environment but a partially adapted mechanical environment. With this in mind, it is plausible that the reported r-squared of values 0.42 and 0.37 could have been even higher it had been possible to correlate an initial mechanical configuration.

The contrasting nature of the correlations presented in this study infers that it is sufficient to base predictions of load-regulated cortical morphology on mechanical data and bone architectures derived from populations of geometrically similar bones. It appears, however, that trabecular bone requires knowledge of a subjects own individual trabecular micro-architecture. To confirm this and to better characterize the relationship between load-regulated bone formation and the mechanical environment, future studies should combine FE analysis with the latest in-vivo imaging techniques. The ability to track changes over shorter periods of time in individual mice by registering sequentially acquired images would enable subject-specific, point-to-point correlation of the mechanical environment and subsequent bone formation activity in 3 dimensions (Schulte, Lambers et al. 2011). Furthermore, mechanical loading alone is not the only factor which affects how bone adapts with time in real-life clinical scenarios. It is likely that synergies exist with other competing bone remodelling stimuli such as age, disease and pharmacological treatments. How these different aspects interact is not yet clear. Mulvihill et al. (Mulvihill and Prendergast 2008) have recently put forward a theoretical framework to explain normal and pathological bone adaptation. Combining the mechanostat model of Frost and certain damage criteria, they assume that the mechanical set points (which determine whether bone is resorbed or formed) change with age or disease. Whilst various attributes of osteoporosis are replicated, the proposed model has not yet been validated. Future studies should therefore address these issues either by designing experiments to test-specific hypotheses.

There are several limitations associated with this study. Firstly, the period of time which the correlations bridge may not be appropriate. Trabecular bone has a much higher turnover rate compared with cortical bone, and it is therefore possible that the initial mechanical environment may be responsible for morphological changes which manifest after only one week, and these changes will in turn alter the mechanical environment resulting in an entirely different pattern of bone formation; hence, the time points we are comparing may be disconnected. Future studies should therefore investigate multiple time points, spanning shorter periods of time using in-vivo micro-computed tomography (Schulte, Lambers et al. 2011). Secondly, the correlations could be significantly influenced by the assumptions upon which the FE models are based. In our FE model, we assume a linearly isotropic material for both cortical and trabecular components, which have a constant and equivalent Young's modulus. In reality, this is not the case owing to the different

degrees of mineralization which are heterogeneously distributed throughout bone (Norman, Shapter et al. 2007). Accounting for this could therefore significantly modify the regional mechanical strain profiles seen in Fig. 3 and therefore alter the correlation between trabecular bone formation and the micro-mechanical environment. This could be compensated for in future studies by creating FE models from grey scale images of bone and assigning different values of Young's moduli to voxels with different grey values. This approach has recently been used as part of an FE-based strategy to enhance the prediction of fracture (MacNeil and Boyd 2008). In this study, the use of multiple Young's moduli to predict structural failure on a global scale yielded minor improvements; nevertheless, this aspect could still have important consequences at a local level. Thirdly, not all forms of potential mechanical stimuli have been accounted for in this study. In focusing on mechanical strain magnitudes, we are considering bone matrix/osteocyte deformation (Robinson, Chatterjee-Kishore et al. 2006; Bonivtch, Bonewald et al. 2007; Vatsa, Breuls et al. 2008; Vatsa, Semeins et al. 2008) as the underlying mechanism which stimulates load-induced bone adaptation. However, it has also been proposed that fluid flow through canaliculi (Zeng, Cowin et al. 1994; Han, Cowin et al. 2004; Price, Zhou et al. 2011) and micro-damage (Burr, Martin et al. 1985; Bentolila, Boyce et al. 1998; Colopy, Benz-Dean et al. 2004) is other potential mechanisms. Future studies should therefore aim to correlate mechanical signals which are representative of these stimuli with load-induced bone adaptation. For example, fluid flow is dependent upon variations in fluid pressure which are induced by variations in structural deformation throughout the bone matrix and could therefore be characterized by mechanical strain gradients.

It should also be pointed out that the dynamic component of the applied load has not been accounted for. This aspect will determine the magnitude of the response (Robling, Hinant et al. 2002; Warden and Turner 2004; Rubin, Judex et al. 2006; Xie, Jacobson et al. 2006). Thus, to enable the prediction of adaptation resulting from loads with different dynamic components, future work should aim to incorporate the effect of frequency and the number of cycles into the description of the 'initial' mechanical environment. In the case of micro-damage-stimulated remodelling, this may be achieved incorporating fatigue data into the FE model (Prendergast and Taylor 1994) or in the case of fluid flow-stimulated remodelling by defining a porous material (Adachi, Kameo et al. 2010).

Finally, in considering strain-based adaptive mechanisms, we have not investigated all possible mechanical parameters. Other parameters which have been correlated in other studies should also be checked for trabecular bone. For example, Carpenter et al (Carpenter and Carter 2008) found that predictions of cortical geometries were enhanced when including tensile strains perpendicular to the periosteal surface into their bone remodelling algorithm.

In this study, we have shown that average, load-induced increases in cortical bone morphology in mechanically loaded B6 caudal vertebrae can be predicted using static finite element models, which describe the typical distribution of mechanical strains for groups of mice sacrificed prior to loading. Conversely, we have also shown that this is not possible to predict load-regulated adaptation in trabecular bone. These results indicate that load-induced cortical morphology can be predicted from population data, whereas the prediction of trabecular morphology requires subject-specific micro-architecture. This may have significant implications for future strategies which aim to improve the prediction of fractures by incorporating load-induced changes in bone. To confirm this, further studies which are longitudinal in design and which exploit the latest in-vivo imaging technologies are proposed.

References

Adachi T, Kameo Y et al (2010) Trabecular bone remodelling simulation considering osteocytic response to fluid-induced shear stress. Philos Trans A Math Phys Eng Sci 368(1920):2669–2682

Bentolila V, Boyce TM et al (1998) Intracortical remodeling in adult rat long bones after fatigue loading. Bone 23(3):275–281

Biewener AA, Fazzalari NL et al (1996) Adaptive changes in trabecular architecture in relation to functional strain patterns and disuse. Bone 19(1):1–8

Bonivtch AR, Bonewald LF et al (2007) Tissue strain amplification at the osteocyte lacuna: a microstructural finite element analysis. J Biomech 40(10):2199–2206

Bouxsein ML, Boyd SK et al (2010) Guidelines for assessment of bone microstructure in Rodents using micro-computed tomography. J Bone Miner Res 25(7):1468–1486

Boyd SK, Müller R et al (2002) Mechanical and architectural bone adaptation in early stage experimental osteoarthritis. J Bone Miner Res 17:687–694

Burr DB, Martin RB et al (1985) Bone remodeling in response to in vivo fatigue microdamage. J Biomech 18(3):189–200

Carpenter RD, Carter DR (2008) The mechanobiological effects of periosteal surface loads. Biomech Model Mechanobiol 7(3):227–242

Colopy SA, Benz-Dean J et al (2004) Response of the osteocyte syncytium adjacent to and distant from linear microcracks during adaptation to cyclic fatigue loading. Bone 35(4):881–891

Duncan RL, Turner CH (1995) Mechanotransduction and the functional response of bone to mechanical strain. Calcif Tissue Int 57(5):344–358

Evans WJ (1998) Exercise and nutritional needs of elderly people: effects on muscle and bone. Gerodontology 15(1):15–24

Guo XE, Eichler MJ et al (2002) Quantification of a rat tail vertebra model for trabecular bone adaptation studies. J Biomech 35(3):363–368

Han Y, Cowin SC et al (2004) Mechanotransduction and strain amplification in osteocyte cell processes. Proc Natl Acad Sci USA 101(47):16689–16694

Hilderbrand T (1999) Direct three-demensional morphometric analysis of human cancellous bone: microstructural data from spine, femur, iliac crest and calcaneus. J Bone Miner Res 14:1167–1174

Johnell O, Kanis JA (2006) An estimate of the worldwide prevalence and disability associated with osteoporotic fractures. Osteoporos Int 17(12):1726–1733

Kanis JA, Johnell O (2005) Requirements for DXA for the management of osteoporosis in Europe. Osteoporos Int 16(3):229–238

Kim CH, Takai E et al (2003) Trabecular bone response to mechanical and parathyroid hormone stimulation: the role of mechanical microenvironment. J Bone Miner Res 18(12):2116–2125

Kotha SP, Hsieh YF et al (2004) Experimental and finite element analysis of the rat ulnar loading model-correlations between strain and bone formation following fatigue loading. J Biomech 37(4):541–548

MacNeil JA, Boyd SK (2008) Bone strength at the distal radius can be estimated from high-resolution peripheral quantitative computed tomography and the finite element method. Bone 42(6):1203–1213

Marcus R (1995) Relationship of age-related decreases in muscle mass and strength to skeletal status. J Gerontol A Biol Sci Med Sci 50:86–87

Müller R, Rüegsegger P (1995) Three-dimensional finite element modelling of non-invasively assessed trabecular bone structures. Med Eng Phys 17(2):126–133

Mulvihill BM, Prendergast PJ (2008) An algorithm for bone mechano-responsiveness: implementation to study the effect of patient-specific cell mechanosensitivity on trabecular bone loss. Comput Methods Biomech Biomed Engin 11(5):443–451

Norman J, Shapter JG et al (2007) Micromechanical properties of human trabecular bone: a hierarchical investigation using nano-indentation. J Biomed Mater Res A 87A(1):196–202

Prendergast PJ, Taylor D (1994) Prediction of bone adaptation using damage accumulation. J Biomech 27(8):1067–1076

Price C, Zhou X et al (2011) Real-time measurement of solute transport within the lacunar-canalicular system of mechanically loaded bone: direct evidence for load-induced fluid flow. J Bone Miner Res 26(2):277–285

Robinson JA, Chatterjee-Kishore M et al (2006) Wnt/beta-catenin signaling is a normal physiological response to mechanical loading in bone. J Biol Chem 281(42):31720–31728

Robling AG, Hinant FM et al (2002) Improved bone structure and strength after long-term mechanical loading is greatest if loading is separated into short bouts. J Bone Miner Res 17(8):1545–1554

Rubin C, Judex S et al (2006) Low-level mechanical signals and their potential as a non-pharmacological intervention for osteoporosis. Age Ageing 35:32–36

Sarver JJ, Elliott DM (2005) Mechanical differences between lumbar and tail discs in the mouse. J Orthop Res 23(1):150–155

Schulte FA, Lambers FM et al (2011) In vivo micro-computed tomography allows direct three-dimensional quantification of both bone formation and bone resorption parameters using time-lapsed imaging. Bone 48(3):433–442

Smith IM, Griffiths DV (1998) Programming the finite element method. Wiley, Chichester

Somerville JM, Aspden RM et al (2004) Growth of C57BL/6 mice and the material and mechanical properties of cortical bone from the tibia. Calcif Tissue Int 74(5):469–475

Vatsa A, Breuls RG et al (2008) Osteocyte morphology in fibula and calvaria—Is there a role for mechanosensing? Bone 43(3):452–458

Vatsa A, Semeins CM et al (2008) Paxillin localisation in osteocytes-Is it determined by the direction of loading? Biochem Biophys Res Commun 377(4):1019–1024

Warden SJ, Turner CH (2004) Mechanotransduction in cortical bone is most efficient at loading frequencies of 5–10 Hz. Bone 34(2):261–270

Webster D, Wasserman E et al (2010) Mechanical loading of mouse caudal vertebrae increases trabecular and cortical bone mass-dependence on dose and genotype. Biomech Model Mechanobiol 9(6):737–747

Webster DJ, Morley PL et al (2008) A novel in vivo mouse model for mechanically stimulated bone adaptation–a combined experimental and computational validation study. Comput Methods Biomech Biomed Engin 11(5):435–441

Xie LQ, Jacobson JM et al (2006) Low-level mechanical vibrations can influence bone resorption and bone formation in the growing skeleton. Bone 39(5):1059–1066

Zeng Y, Cowin SC et al (1994) A fiber matrix model for fluid flow and streaming potentials in the canaliculi of an osteon. Ann Biomed Eng 22(3):280–292